

Neutrosophic fusion of multimodal brain images: Integrating neutrosophic entropy and feature extraction

K.G. Lavanya, P. Dhanalakshmi *, M. Nandhini

Department of Applied Mathematics, Bharathiar University, Coimbatore, India

ARTICLE INFO

Keywords:

Multi-modal brain image
Neutrosophic fusion
Neutrosophic entropy
Indeterminacy
Feature extraction
Tamura features

ABSTRACT

Due to the rapid growth of imaging modalities in clinical analysis and the indispensable requirement of brain images from various imaging modalities for diagnosing a disease, multi-modal brain image fusion has become an intriguing problem among researchers. Thus, the main motive of this paper is to obtain all the necessary information about the source images in a single fused image of high contrast with clear boundaries and without unnecessary noise. Accordingly, this paper proposes a new approach to eradicate the indeterministic and uncertainty present in brain images with the benefits of the neutrosophic set. Also, a novel neutrosophic entropy is developed to acquire the accurate edge details of the image. In addition, to extract requisite features from the images, Tamura features are implemented. Finally, the fusion is performed by comparing the extracted feature values from the images. Subsequently, the experiment is conducted with three different sets of brain datasets and compared with six other fusion algorithms to prove the efficiency of the proposed method. To support this, qualitative and quantitative assessments for each dataset are executed, and the results are tabulated. The results clearly show that the information is accurately represented, preserving the curves and edges. Moreover, this algorithm consistently produces the highest metric values and remains reasonably efficient in time consumption, thus balancing performance and efficiency.

1. Introduction

In this contemporary world, imaging technology has shown a steep increase in growth due to the advances in capturing different organ information. There are various imaging technology available with the stipulated applications, and they can be used according to the needs of the radiologist for analyzing the problem. In this aspect, the commonly used imaging technologies are X-rays, computed tomography, magnetic resonance imaging (MRI), positron emission tomography, single-photon emission tomography (SPECT) and so on. Notably, a different sequence of MRI, such as T1-weighted MR, T2-weighted MR, and FLAIR, is also available that differs in the radio frequency, and these have peculiar applications in characterizing the tissues. All these imaging modalities have many advantages with some limitations. In this concern, the advantages and limitations of the imaging technologies considered in this paper are tabulated below (see Table 1). From the table, it is perceived that all imaging modalities are unavoidable, despite their limitations. Also, sometimes clinicians require both the anatomical and functional details for the etiological analysis of the disease. Thus, this paves the way for medical computer-aided image fusion which gains the advantages of imaging modalities in a single image [1]. Consequently, it improves diagnostic precision and provides unbiased

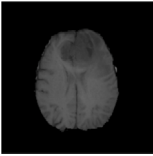
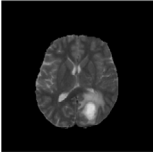
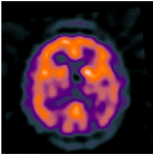
decisions [2]. Due to these properties, they are applied in various areas such as neurological research, lesion examination, etc. Further, all the images obtained from various imaging technologies require separate high storage capacity for each image; thus, a fusion of those images aids in reducing the storage capacity. On the whole, medical image fusion provides a single high-resolution image from complementary low-resolution images with all the requisite information rather than redundant information at a low storage cost [3].

In literature, there are three levels of image fusion available, namely pixel-level fusion, feature-level fusion and decision-level fusion. Mainly, the pixel-level fusion is divided into two categories: spatial domain and transform domain. In the spatial domain, simple operators such as minimum, maximum and rank methods are used to fuse the source images. These methods suffer from large spectral degradation. Also, statistical methods such as principal component analysis, independent component analysis [4] and linear discriminant analysis are classified under a spatial domain. However, these methods are sensitive to variations in illuminations. While considering the transform domain, it is further divided into multi-resolution analysis (MRA) methods and multi-scale analysis (MSA) methods. The MRA method includes the simple transform methods, like the pyramid decomposition method, wavelet transformation methods such as discrete wavelet

* Corresponding author.

E-mail address: ghanamath@buc.edu.in (P. Dhanalakshmi).

Table 1
Advantages and limitations of imaging modalities.

Imaging modalities	Images	Advantages	Limitations
T1-weighted MR		Responsive for the analysis of soft tissues and portrays the inflammation.	The abnormalities in the tissues are not detected properly.
T2-weighted MR		Highly sensitive for soft tissues and shows the thickness of tumor.	Poorly concentrates on non-invasive diseases.
SPECT		Interprets the metabolic activity of cells and characterizes the tumor.	Gives images with very low resolution.

transform [5], multi wavelet transform, dual-tree complex wavelet transform [6], lifting wavelet transform and empirical mode decomposition [7]. All these methods need more shift-invariance and directionality. Then, in the MSA method, transformations such as curvelet transform, contourlet transform, and shearlet transform [8] are available. The above-mentioned methods alter the spectral information and introduce artifacts.

In addition to the above fusion methods, there is some requirement for strategical methods which inspect the medical images and provide the result according to it. In this aspect, some strategical fusion methods developed now are guided filtering techniques [9], fuzzy methods, dictionary learning methods, sparse representation [10], and neural networks [11]. Among them, the fuzzy methods contribute more to medical image fusion since medical images are usually vague. The fuzzy set was initially proposed by Zadeh in the year 1965 to deal with uncertain data [12]. In image fusion, the fuzzy set (FS) gives the degree of belongingness for a pixel in the image, and fusion takes place accordingly. Many fuzzy image fusion algorithms are present in the literature. Manchanda et al. used fuzzy transform to handle the data loss of the error image and then fused the image with precision [13]. However, sometimes, there is a dilemma in choosing the membership function for fuzzy image fusion, and the requirement to study the hesitancy in assigning the membership function has arisen. In that case, the generalization of FS called intuitionistic fuzzy set (IFS) developed by Atanassov [14] in 1983 can be used. Thus, three aspects to analyze the uncertain image are involved: membership degree, non-membership degree and hesitation degree. By considering this ideology, many authors proposed a fusion algorithm using IFS. Tirupal et al. framed IFS based medical image fusion that is obtained from a Sugeno generator and eradicated the noise present in the image [15]. But, here, the hesitation degree depends on the membership and non-membership degree. Nevertheless, in some incomplete problems, there is a need to find the indeterminate value without the aid of membership and non-membership functions. Therefore, Smarandache, in 1998, introduced the neutrosophic set (NS), which is the generalization of FS and IFS [16]. NS has three independent membership functions to determine the inherent uncertainty of data: truth, false and indeterminacy membership functions. These are defined on the non-standard unit interval $[0^-, 1^+]$, which cannot be applied to real-life problems. To eradicate this issue, in 2005, Wang et al. introduced the concept of a single-valued neutrosophic set (SVNS), defined on the standard interval $[0, 1]$ [17]. For simplicity, the SVNS is always referred to as NS in real-world problems. Thus, NS is implemented by many researchers in processing the

indeterministic properties of medical images. In particular, Premalatha and Dhanalakshmi proposed the fusion algorithm to merge the MRI brain images using the NS and evaluated the algorithm in objective and subjective aspects [18].

This paper mainly concentrates on the fusion of brain images from various medical imaging modalities. The motivation to consider brain images for fusion is because it is a delicate and complicated organ with many neurons, up to 100 billion. Therefore, it is necessary to study the inter and intra cerebral problems with attention since some may lead to death [19]. Three main issues that cause problems in fusing multimodal brain images are impreciseness, unclear edges and indistinguishable features. The first issue, vagueness and impreciseness with noise, is due to the limiting factors of imaging modalities. Thus, it can be handled effectively using NS for brain image fusion. The second issue in fusing the brain images is to optimally produce the edges of the source images without any deterioration. For this purpose, neutrosophic entropy is used, which is the measure of imperfection in the set. Majumdar and Samantha [20] initially gave the axiomatic definition of neutrosophic entropy, and then many authors devised neutrosophic entropy according to their usage. Pritpal Singh devised a neutrosophic entropy-based clustering algorithm to segment Parkinson's disease [21]. Then, Bian et al. used neutrosophic entropy to segment the melanoma images [22]. Then, the third issue can be resolved by implementing feature extraction, which has a significant responsibility in distinguishing the normal tissues from the affected tissues in the brain. Especially, texture feature tends to group similar and recurring pattern in the brain image. Many texture feature extraction methods are available in the literature, such as gray level co-occurrence matrix [23], Local binary pattern, wavelet methods, etc. To be specific, the Tamura texture feature [24] is the statistical approach to determine the psychophysical structures. This feature includes coarseness, contrast, directionality, line-likeness, regularity and roughness, and many researchers utilized this to fuse images. Xiaoming et al. employed Tamura features and the wavelet transform to extract the features and then used the Hausdorff distance to measure similarity [25].

Based on the analysis, first, the proposed method involves a transformation of crisp brain images into a neutrosophic domain (comprising truth, false, and indeterminate values) to assess impreciseness within the source images. Next, a unique neutrosophic entropy is devised to enhance fusion while preserving contour details. This novel approach utilizes the truth, false, and indeterminate values derived from the neutrosophic domain to generate a neutrosophic entropy image. Subsequently, the fusion process follows two tracks to produce the final

fused image: one emphasizes high contrast and noise reduction, and the other focuses on detailed contour information. This is achieved by extracting features from the obtained truth image (containing absolute information) and the neutrosophic entropy image (highlighting edge details). Therefore, Tamura's coarseness and contrast features are utilized for the truth and neutrosophic entropy images, respectively. Thus, the coarseness feature value is employed to merge the truth images of the source images, while the contrast feature value is used to blend the neutrosophic entropy images of the source images. Consequently, the two resulting fused images are combined into a single comprehensive image. This integrated image encapsulates all necessary information from the source images, including contour details, while ensuring freedom from unwanted artifacts. Experimental trials are carried out to evaluate the effectiveness and performance of the proposed algorithm. The significant contribution of the proposed framework is given below:

- (i) The brain images from medical imaging modalities are usually incomplete and indeterministic. This state of brain images is addressed effectively by using NS; so that the misleading of the fusion process is avoided.
- (ii) A novel neutrosophic entropy is framed with all three NS domains to fetch the minuscule edge details of the brain image. This aids in merging the information of brain images with curves and contour details.
- (iii) Coarseness and contrast features are extracted from the truth and neutrosophic entropy image. Thus, the decision to fuse the brain images is taken using these feature values.

The remaining part of the manuscript is arranged as follows: Section 2 presents the basic concepts needed for this work. In Section 3, the proposed methodology with the framework of novel neutrosophic entropy is delineated. Then, the experimental results and analysis are given in Section 4. Finally, Section 5 illustrates the conclusion of this work and future direction is also provided.

2. Conceptual basis

The notable definitions and the required theoretical concepts to decipher the proposed neutrosophic entropy and Tamura-feature based multi-modal medical image fusion (NETMMF) method are given in this section.

Definition 1 (NS). [16] Let \mathcal{Z} be the universal set and the neutrosophic set \mathcal{N} in \mathcal{Z} is represented by using the neutrosophic components such that $\mathcal{N} = \{ \langle \mathcal{T}_{\mathcal{N}}(z), \mathcal{I}_{\mathcal{N}}(z), \mathcal{F}_{\mathcal{N}}(z) \rangle \mid z \in \mathcal{Z} \}$ where $\mathcal{T}_{\mathcal{N}}(z)$, $\mathcal{I}_{\mathcal{N}}(z)$, $\mathcal{F}_{\mathcal{N}}(z)$ denotes the truth, indeterminacy and falsity membership function respectively and it is defined on the standard and the non-standard unit interval $]0^-, 1^+[$ with the condition $0^- \leq \mathcal{T}_{\mathcal{N}}(z) + \mathcal{I}_{\mathcal{N}}(z) + \mathcal{F}_{\mathcal{N}}(z) \leq 3^+$.

Definition 2 (SVNS). [17] SVNS is the direct outcome of NS which is defined on the standard unit interval $[0, 1]$ with the condition $0 \leq \mathcal{T}_{\mathcal{N}}(z) + \mathcal{I}_{\mathcal{N}}(z) + \mathcal{F}_{\mathcal{N}}(z) \leq 3$. Let \mathcal{Z} be the finite universal set such that $\mathcal{Z} = \{z_1, z_2, \dots, z_n\}$. If \mathcal{Z} is continuous, then for each element \mathcal{Z} in SVNS can be expressed as

$$\mathcal{N} = \int_{\mathcal{N}} \langle \mathcal{T}_{\mathcal{N}}(z), \mathcal{I}_{\mathcal{N}}(z), \mathcal{F}_{\mathcal{N}}(z) \rangle / z, z \in \mathcal{Z} \quad (1)$$

Similarly, if \mathcal{Z} is discrete, then for each element \mathcal{Z} in SVNS can be indicated as

$$\mathcal{N} = \sum_{i=1}^n \langle \mathcal{T}_{\mathcal{N}}(z_i), \mathcal{I}_{\mathcal{N}}(z_i), \mathcal{F}_{\mathcal{N}}(z_i) \rangle / z_i, z_i \in \mathcal{Z}. \quad (2)$$

Definition 3 (Neutrosophic image). [26] Let S be the classical source image of dimension $A \times B$ with L level of grayness. Then, any pixel $S(q, r)$ can be converted into neutrosophic image ($S_{\mathcal{N}}$) as given below

$$S_{\mathcal{N}} : A \times B \xrightarrow{S(q,r)=gl} G \xrightarrow{\mathcal{T}_S(gl), \mathcal{I}_S(gl), \mathcal{F}_S(gl)} [0, 1]$$

where $\mathcal{T}_S(gl)$, $\mathcal{I}_S(gl)$, $\mathcal{F}_S(gl)$ denotes the belongingness, indeterminacy and non-belongingness membership values of the image. First, to determine the truth membership, the local mean value \overline{gl} is computed, which is given as

$$\overline{gl}(q, r) = \frac{1}{win \times win} \sum_{a=q-\frac{win}{2}}^{q+\frac{win}{2}} \sum_{b=r-\frac{win}{2}}^{r+\frac{win}{2}} gl(a, b)$$

where $win \times win$ denotes the size of the window and the pixel value at $(a, b)^{th}$ location is notated as $gl(a, b)$. Therefore, the truth membership is evaluated by

$$\mathcal{T}_S(S(q, r)) = \frac{\overline{gl}(q, r) - \overline{gl}_{min}}{\overline{gl}_{max} - \overline{gl}_{min}} \quad (3)$$

such that \overline{gl}_{max} , \overline{gl}_{min} refers to the maximum and minimum value of $\overline{gl}(q, r)$. Second, to determine the indeterminacy membership value of the image, the absolute value is found such that

$$\eta(q, r) = abs(\overline{gl}(q, r) - \overline{gl}(q, r))$$

Then, the indeterminacy membership value is given as

$$\mathcal{I}_S(S(q, r)) = \frac{\eta(q, r) - \eta_{min}}{\eta_{max} - \eta_{min}} \quad (4)$$

where η_{max} , η_{min} is the maximum and minimum value of $\eta(q, r)$. Lastly, the falsity membership value of the image is determined as

$$\mathcal{F}_S(S(q, r)) = 1 - \mathcal{T}_S(S(q, r)) \quad (5)$$

To conclude, the domain of neutrosophic image is given as follows

$$S_{\mathcal{N}} = \left\{ \langle S(q, r), \mathcal{T}_S(S(q, r)), \mathcal{I}_S(S(q, r)), \mathcal{F}_S(S(q, r)) \rangle ; 0 \leq q \leq A-1, \right. \\ \left. 0 \leq r \leq B-1, 0 \leq S(q, r) \leq L-1, 0 \leq \mathcal{T}_S, \mathcal{I}_S, \mathcal{F}_S \leq 1 \right\}$$

Definition 4 (Neutrosophic entropy). The entropy is utilized to quantify the uncertainty present in the set. Since SVNS deals with the uncertainty of the data like FS and IFS, the computation of their uncertainty is attainable. The higher the value of the entropy represents the likeness for the probability of intensity with even distribution and vice-versa. Therefore, the entropy of SVNS can be defined as $ENT : \mathcal{N} \rightarrow [0, 1]$ which fulfills the following axioms [20]

- (i) $ENT(\mathcal{P}) = 0 \iff \mathcal{P}$ is crisp set.
- (ii) $ENT(\mathcal{P}) = 1 \iff \mathcal{T}_{\mathcal{P}}(z) = \mathcal{F}_{\mathcal{P}}(z)$ and $\mathcal{I}_{\mathcal{P}}(z) = 0.5, \forall z \in \mathcal{Z}$ ($\because \mathcal{T}_{\mathcal{P}}(z) = 1 - \mathcal{F}_{\mathcal{P}}(z)$).
- (iii) $ENT(\mathcal{P}) \geq ENT(\mathcal{Q}) \iff \mathcal{P}$ is more uncertain than \mathcal{Q} . (ie.) $|\mathcal{T}_{\mathcal{P}}(z) - \mathcal{F}_{\mathcal{P}}(z)| \leq |\mathcal{T}_{\mathcal{Q}}(z) - \mathcal{F}_{\mathcal{Q}}(z)|$ and $|\mathcal{I}_{\mathcal{P}}(z) - \mathcal{I}_{\mathcal{P}^c}(z)| \leq |\mathcal{I}_{\mathcal{Q}}(z) - \mathcal{I}_{\mathcal{Q}^c}(z)|$.
- (iv) $ENT(\mathcal{P}) = ENT(\mathcal{P}^c), \forall \mathcal{P} \in \mathcal{N}$.

Definition 5 (Tamura-feature). Tamura feature extraction consists of six items considered mandatory features in an image. In this work, two components are taken into account among them, namely, coarseness and contrast [24]. As discussed in the Definition 3, consider an image S of dimension $A \times B$. Then, the coarseness of an image is calculated as follows

(a) Coarseness

The mean at each pixel with neighborhood of size $2^m \times 2^m$ is computed as follows

$$Mean_m(q, r) = \sum_{a=q-2^{m-1}}^{q+2^{m-1}-1} \sum_{b=r-2^{m-1}}^{r+2^{m-1}-1} \frac{gl(a, b)}{2^{2m}}$$

From this, the horizontal and vertical parts are computed with the difference between mean intensity $Mean_m$ of the non-overlapping neighborhood.

$$D_{m,h}(q, r) = |Mean_m(q + 2^{m-1}, r) - Mean_m(q - 2^{m-1}, r)|$$

and,

$$D_{m,v}(q, r) = |Mean_m(q, r + 2^{m-1}) - Mean_m(q, r - 2^{m-1})|$$

Thus, $\max_{1 \leq m \leq L} (D_{m,h}(q, r), D_{m,v}(q, r))$ is selected such that the optimal size of each pixel O_{best} is calculated as

$$O_{best}(q, r) = 2^m \quad (6)$$

Finally, the coarseness feature is estimated as the average of O_{best} , which is given as

$$Coarseness(S) = \frac{1}{A \times B} \sum_{a=0}^{A-1} \sum_{b=0}^{B-1} O_{best}(a, b) \quad (7)$$

(b) Contrast

The contrast feature of an image can be measured using the following equation

$$Contrast(S) = \frac{\sigma}{(\mu^4 / \sigma^4)^n} \quad (8)$$

where, σ be the standard deviation, the term (μ^4 / σ^4) is called the kurtosis such that μ^4 is the fourth moment about mean and σ^4 is the square of variance and n is any positive integer to be determined.

3. The proposed NETMMF fusion method

This section delineates the proposed fusion method for multi-modal medical image fusion. As examined in the introduction 1, the multi-modal medical image fusion is a complicated field in the research area which needs careful examination. The fused medical image is the single image obtained from the collection of two or more low-resolution medical images, and the obtained outcome must be in high resolution with a substantial number of relevant information such that no artifacts are included. The main focus of the medical image fusion algorithm is to transfer information with edge details. For this purpose, a novel neutrosophic entropy is developed, which yields the appropriate detailing of the edge. The formation of the novel entropy with examples is elucidated in the subsection.

3.1. A novel neutrosophic entropy for fusion

The entropy for the SVNS is developed such that it satisfies the axioms given in Definition 4. Thus, the neutrosophic entropy is established through the theorem provided below.

Theorem 1. Consider a finite domain $\mathcal{Z} = \{z_1, z_2, \dots, z_n\}$ and $\mathcal{P} = \{z_i, \langle \mathcal{T}_p(z_i), \mathcal{I}_p(z_i), \mathcal{F}_p(z_i) \rangle \mid z_i, z_i \in \mathcal{Z}\}$ be SVNS. If

$$ENT(\mathcal{P}) = \frac{1}{n} \sum_{i=1}^n \left[1 - \sqrt{|\mathcal{T}_p(z_i) - \mathcal{F}_p(z_i)| |\mathcal{I}_p(z_i) - \mathcal{I}_{p^c}(z_i)|} \right] \quad (9)$$

for all $z_i \in \mathcal{Z}$, then $ENT(\mathcal{P})$ is an entropy of SVNS.

Proof. The theorem is proved using the axiomatic conditions given in Definition 4.

- (i) Consider \mathcal{P} as a crisp set. Then, either $(\mathcal{T}_p(z_i), \mathcal{I}_p(z_i), \mathcal{F}_p(z_i)) = (0, 0, 1)$ or $(\mathcal{T}_p(z_i), \mathcal{I}_p(z_i), \mathcal{F}_p(z_i)) = (1, 0, 0)$, $\forall z_i \in \mathcal{Z}$. Thus, it is obvious that $ENT(\mathcal{P}) = 0$.

- (ii) If $(\mathcal{T}_p(z_i), \mathcal{I}_p(z_i), \mathcal{F}_p(z_i)) = (0.5, 0.5, 0.5) \forall z_i \in \mathcal{Z}$. Then,

$$ENT(\mathcal{P}) = \frac{1}{n} \sum_{i=1}^n \left[1 - \sqrt{|0.5 - 0.5| |0.5 - 0.5|} \right]$$

Thus, it is clear that $ENT(\mathcal{P}) = 1$.

- (iii) Let $|\mathcal{T}_p(z_i) - \mathcal{F}_p(z_i)| = p$, $|\mathcal{T}_Q(z_i) - \mathcal{F}_Q(z_i)| = q$, $|\mathcal{I}_p(z_i) - \mathcal{I}_{p^c}(z_i)| = \gamma$, $|\mathcal{I}_Q(z_i) - \mathcal{I}_{Q^c}(z_i)| = \mu$. Also, $p \leq q$ and $\gamma \leq \mu$. Then,

$$\begin{aligned} ENT(\mathcal{P}) - ENT(\mathcal{Q}) &= \frac{1}{n} \sum_{i=1}^n \left[\left(1 - \sqrt{|\mathcal{T}_p(z_i) - \mathcal{F}_p(z_i)| |\mathcal{I}_p(z_i) - \mathcal{I}_{p^c}(z_i)|} \right) - \left(1 - \sqrt{|\mathcal{T}_Q(z_i) - \mathcal{F}_Q(z_i)| |\mathcal{I}_Q(z_i) - \mathcal{I}_{Q^c}(z_i)|} \right) \right] \end{aligned}$$

$$\begin{aligned} \therefore ENT(\mathcal{P}) - ENT(\mathcal{Q}) &= \frac{1}{n} (1 - \sqrt{p\gamma} - 1 + \sqrt{q\mu}) \\ &= \frac{1}{n} (\sqrt{p\gamma} - \sqrt{q\mu}) \end{aligned}$$

As $p \leq q$ and $\gamma \leq \mu$, it is obvious that $p\gamma \leq q\mu$ and it follows $\sqrt{p\gamma} \leq \sqrt{q\mu}$. Therefore, $ENT(\mathcal{P}) \geq ENT(\mathcal{Q})$.

- (iv) It is known that, $\mathcal{T}_{p^c}(z_i) = \mathcal{F}_p(z_i)$, $(\mathcal{I}_{p^c}(z_i))^c = \mathcal{I}_p(z_i)$, $\mathcal{F}_{p^c}(z_i) = \mathcal{T}_p(z_i)$. Thus, $ENT(\mathcal{P}) = ENT(\mathcal{P}^c)$ is obvious.

This completes the proof.

Example 1. Suppose $\mathcal{Z} = \{z_1, z_2, z_3, z_4\}$ be the universal set and \mathcal{N} be SVNS in \mathcal{Z} defined as

$$\mathcal{N} = \left\{ \frac{z_1}{\langle 0.73, 0.54, 0.27 \rangle}, \frac{z_2}{\langle 0.45, 0.68, 0.55 \rangle}, \frac{z_3}{\langle 0.82, 0.57, 0.18 \rangle}, \frac{z_4}{\langle 0.67, 0.81, 0.33 \rangle} \right\}$$

Then, $ENT(\mathcal{N}) = 0.7151$. Thus, $ENT(\mathcal{N}) \in [0, 1]$.

3.2. Proposed methodology

The design of the proposed NETMMF method is described in this part. The NETMMF method aims to provide a sharp fused image without uncertainty such that the small edge details are preserved, and the visual consistency is improved. The schematic representation of the proposed NETMMF method is given in Fig. 1. Let us consider two pre-registered medical images M_1 and M_2 of dimension $A \times B$ with L level of grayness. The gray-level of the images M_i at the position (a, b) is represented as the gray-level matrix such that

$$G_i = \begin{pmatrix} gl_i(1, 1) & gl_i(1, 2) & \dots & gl_i(1, b) \\ gl_i(2, 1) & gl_i(2, 2) & \dots & gl_i(2, b) \\ \vdots & \vdots & \ddots & \vdots \\ gl_i(a, 1) & gl_i(a, 2) & \dots & gl_i(a, b) \end{pmatrix} \quad (10)$$

Usually, the medical images are uncertain and have low illumination with poor contrast. In this connection, the neutrosophic set is used to handle the situation better and to avoid the misconception of taking a pixel as a grayness or edges. Accordingly, the gray-level matrix in the Eqs. (10) is converted to a neutrosophic image matrix. If $gl_i(a, b)$ is the gray-level value, then the corresponding neutrosophic membership values of the gray-level, $nd_i(a, b) \in \langle \mathcal{T}_{G_i}(G_i(q, r)), \mathcal{I}_{G_i}(G_i(q, r)), \mathcal{F}_{G_i}(G_i(q, r)) \rangle$ is evaluated by the Eqs. (3)–(5). Hence, the neutrosophic image matrix is as follows

$$NM_i = \begin{pmatrix} nd_i(1, 1) & nd_i(1, 2) & \dots & nd_i(1, b) \\ nd_i(2, 1) & nd_i(2, 2) & \dots & nd_i(2, b) \\ \vdots & \vdots & \ddots & \vdots \\ nd_i(a, 1) & nd_i(a, 2) & \dots & nd_i(a, b) \end{pmatrix} \quad (11)$$

From the above-defined neutrosophic image matrix, three separate image domains are obtained: truth, indeterminacy and falsity image. The truth membership image contains the absolute image with textual information and well-defined bright regions. Whereas the falsity membership image interprets the dark regions and the pixel values, which cannot be determined correctly is portrayed in the indeterminacy membership image. To perceive this concept, the truth, the indeterminacy and the falsity membership images are shown in schematic representation (see Fig. 1).

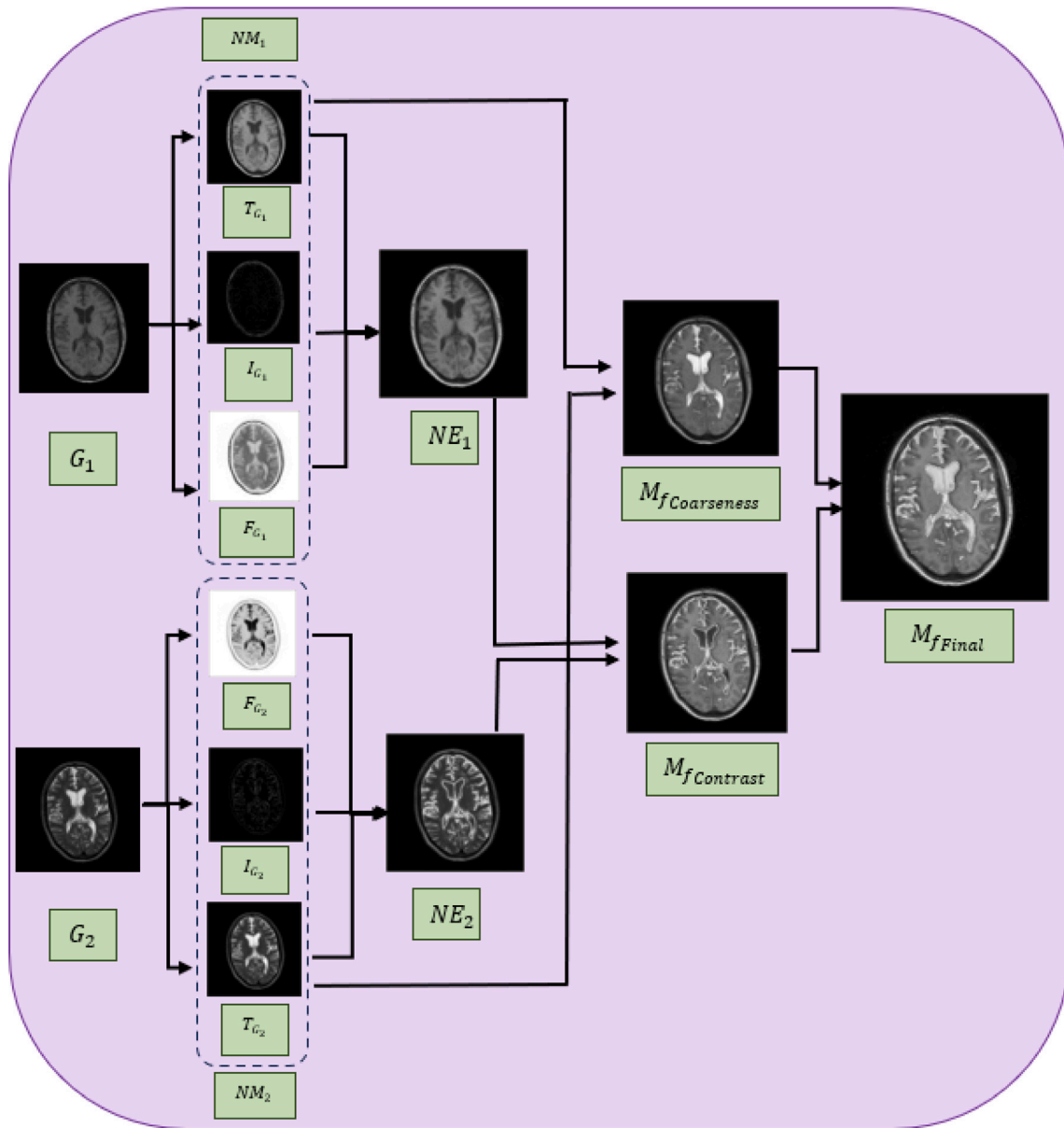


Fig. 1. Schematic representation of the proposed NETMMF algorithm.

Next, the edge information of the source images must be transferred to the fused image without degrading the gray value. On that account, the developed neutrosophic entropy provided in (9) is applied to each pixel of the matrices given in (11). Thus, the neutrosophic entropy matrix is as below

$$NE_i = \begin{pmatrix} ENT(nd_i(1,1)) & ENT(nd_i(1,2)) & \dots & ENT(nd_i(1,b)) \\ ENT(nd_i(2,1)) & ENT(nd_i(2,2)) & \dots & ENT(nd_i(2,b)) \\ \vdots & \vdots & \ddots & \vdots \\ ENT(nd_i(a,1)) & ENT(nd_i(a,2)) & \dots & ENT(nd_i(a,b)) \end{pmatrix}, \quad (12)$$

Thus, the entropy matrix provides the appropriate edge details of the source image, which benefits the upcoming fusion process. After that, feature extraction is the significant process in the medical image fusion method. The feature extraction methods collect the meaningful regions according to the mentioned feature and aid in merging the images. As stated before, Tamura's coarseness and contrast feature is considered in this work. First, the coarseness feature is implemented to the truth image since the absolute amount of information is present in

it. Thus, it contributes in extracting spectral information without any degradation. Next, the contrast feature is applied to the entropy image to obtain the minuscule edges. Thereby, the truth and entropy image matrix is subdivided into blocks of $s \times t$ dimension such that $T_{G_{ij}}$ and NE_{ij} denotes the j th block of truth and entropy image matrix. So, as pointed out earlier, the coarseness feature is applied to each block of the truth image $T_{G_{ij}}$ such that

$$Coarseness_{ij} = \frac{1}{s \times t} \sum_{a=0}^{s-1} \sum_{b=0}^{t-1} O_{ij_{best}}(a,b) \quad (13)$$

where $O_{ij_{best}}$ is calculated for each block of $T_{G_{ij}}$ as given in Eq. (6). Similarly, the contrast feature is applied to each block of the neutrosophic image NE_{ij} such that

$$Contrast_{ij} = \frac{\sigma_{ij}}{(\mu_{ij}^4 / \sigma_{ij}^4)^n} \quad (14)$$

where the variables are as given in Eq. (8) that is calculated for NE_{ij} . The next level of the process is to fuse the images according to the

obtained feature values of each block. Hence, the fused blocks acquired using the coarseness feature for the truth image are given below

$$M_{f_j} = \begin{cases} \mathcal{T}_{G_{1j}}(a, b), & \text{if } Coarseness_{1j} > Coarseness_{2j} \\ \mathcal{T}_{G_{2j}}(a, b), & \text{if } Coarseness_{1j} < Coarseness_{2j} \\ \frac{\mathcal{T}_{G_{1j}}(a, b) + \mathcal{T}_{G_{2j}}(a, b)}{2}, & \text{Otherwise} \end{cases} \quad (15)$$

Likewise, the fused blocks obtained using the contrast feature for entropy image are as follows

$$M_{f_j} = \begin{cases} NE_{1j}(a, b), & \text{if } Contrast_{1j} > Contrast_{2j} \\ NE_{2j}(a, b), & \text{if } Contrast_{1j} < Contrast_{2j} \\ \frac{NE_{1j}(a, b) + NE_{2j}(a, b)}{2}, & \text{Otherwise} \end{cases} \quad (16)$$

Now, the disintegrated blocks M_{f_j} and M_{f_j} are reconstructed into images $M_{f_{Coarseness}}$ and $M_{f_{Contrast}}$ respectively. Therefore, both the textural and edge details are separately obtained through the fused images $M_{f_{Coarseness}}$ and $M_{f_{Contrast}}$. Next, these two fused images are merged as a single image that carries all the significant information with minute details. This process is executed by counting the number of blackness BR and whiteness WR in each blocks M_{f_j} and M_{f_j} . Hence, the final fused image is obtained by using the equation mentioned below

$$M_{f_j} = \begin{cases} \min(M_{f_j}, M_{f_j}), & \text{if } BR > WR \\ \max(M_{f_j}, M_{f_j}), & \text{if } BR < WR \\ \frac{M_{f_j} + M_{f_j}}{2}, & \text{Otherwise} \end{cases} \quad (17)$$

Reconstruct the blocks into fused image $M_{f_{Final}}$ and it must be converted again into a crisp image for analysis purposes. Accordingly, the de-neutrosophication of the fused image is carried out using the equation

$$M_D = g_{max}^I - g_{min}^I * M_{f_{Final}} + g_{min}^I \quad (18)$$

Thus, the proposed medical image fusion is described in detail. The algorithm of the proposed NETMMF method is given in Algorithm 1.

Algorithm 1 Flow of proposed NETMMF algorithm

Require: Two medical images M_1 and M_2 of dimension $A \times B$, the size of the blocks $s \times t$, the window size win to compute local mean value, the neighborhood sizes $2^m \times 2^m$.

- Step 1:** Obtain the gray-level images G_i for the source images M_i using the equation (10).
- Step 2:** Compute the neutrosophic image matrix NM_i by the equation (11) such that each $nd_i(a, b) \in \langle \mathcal{T}_{G_i}(G_i(q, r)), \mathcal{I}_{G_i}(G_i(q, r)), \mathcal{F}_{G_i}(G_i(q, r)) \rangle$.
- Step 3:** Evaluate the neutrosophic entropy matrix NE_i as mentioned in the equation (12).
- Step 4:** Disintegrate the truth matrix and neutrosophic entropy matrix into blocks as $\mathcal{T}_{G_{ij}}$ and NE_{ij} .
- Step 5:** Determine the coarseness feature $Coarseness_{ij}$ for the blocks of truth matrix by the formula as in equation (13).
- Step 6:** Measure the contrast feature $Contrast_{ij}$ for the blocks of entropy matrix as given in equation (14).
- Step 7:** Obtain the fused truth M_{f_j} and entropy M_{f_j} blocks by using the equations (15) & (16).
- Step 8:** Reconstruct the fused blocks into fused images as $M_{f_{Coarseness}}$ and $M_{f_{Contrast}}$.
- Step 9:** Evaluate the final fused block M_{f_j} using the equation (17).
- Step 10:** Finally, the reconstruct the blocks into image $M_{f_{Final}}$ and de-neutrosophication process is executed as in the formula (18).

4. Experimental study

In this section, the study to examine the effectiveness of the proposed NETMMF is provided. The description about the materials to execute the algorithm, comparative benchmarking fusion methods, fusion metrics is given in detail.

4.1. Experimental arrangement

Three categories of brain image datasets are assessed to investigate the diversity of the proposed NETMMF method in aspects of varying dimensions, intensity and disease types of brain image. In this regard, the dataset-1 is taken from the BraTS datasets [27] which contains glioma type of brain tumor images obtained from four imaging modalities. This work examines the fusion of T1-weighted MR and T2-weighted MR glioma images. It contains images in MetaImage format with dimension 240×240 . The dataset-2 consists of T1-weighted MR and T2-weighted MR brain images for multiple sclerosis disease, available in [28]. The images in this dataset are of NiftI format with 256×256 dimension. Then, the brain images of Alzheimer's disease are considered as the dataset-3, which is accessed from the whole brain atlas offered by Harvard University [29]. GIF format images of SPECT and T2-weighted MR modalities are collected with 256×256 dimension. The experiment is done for more than 100 images from these datasets using MATLAB 2019a software, but by considering the paper format, results for sample pairs of each dataset are given in this work (see Fig. 2).

4.2. Comparative fusion methods

Six other benchmarking fusion methods for multi-modal medical image fusion are considered to test the potency of the proposed fusion method in merging the multi-modal medical image fusion. First, one of the statistical fusion methods developed by Panda and Agrawal [4], known as the EBFS-ICA fusion algorithm, is considered to fuse medical images. Second, NSST with pulse-coupled neural network (BM-PCNN-NSST) fusion technique devised by Tan et al. [8] is taken. The third fusion method is based on the sparse representation using morphological component analysis (CS-MCA) that is proposed by Liu et al. [10]. Then, the fourth image fusion method taken is pioneered by Xie et al. in which multi-channel bi-dimensional empirical mode decomposition based on the morphological filter (MF-MBEMD) is used to integrate the images [7]. Afterwards, the sixth fusion algorithm employs fast-guided filtering and an extended difference-of-Gaussians (FGF-XDoG) technique proposed by Jie et al. [9]. Lastly, the image fusion method devised by Tirupal is considered, in which the Sugeno type generator is used to fuse the images via an intuitionistic fuzzy set (SIFS) [15]. All the parameters are as it is prescribed in the respective papers. Also, it is noted that one method from each fusion type, as discussed in the introduction 1, is taken as the state-of-the-art method.

4.3. Fusion metrics

Some of the statistical metrics for fusion are available in the literature to validate the outcome of the fusion result. Here, standard deviation, universal image quality index, peak signal-to-noise ratio (PSNR), structural similar index measure and feature mutual index are used to analyze the fusion results. All these metrics describe peculiar information about the output image. The formula for each metric is given below.

1. Standard deviation (SD)

The SD [30] portrays the contrast and brightness preservation of the fused image. The higher value of this metric resembles the good fused image. It is given as

$$SD = \sqrt{\frac{1}{A \times B} \sum_{a=1}^A \sum_{b=1}^B (M_D(a, b) - Mean)} \quad (19)$$

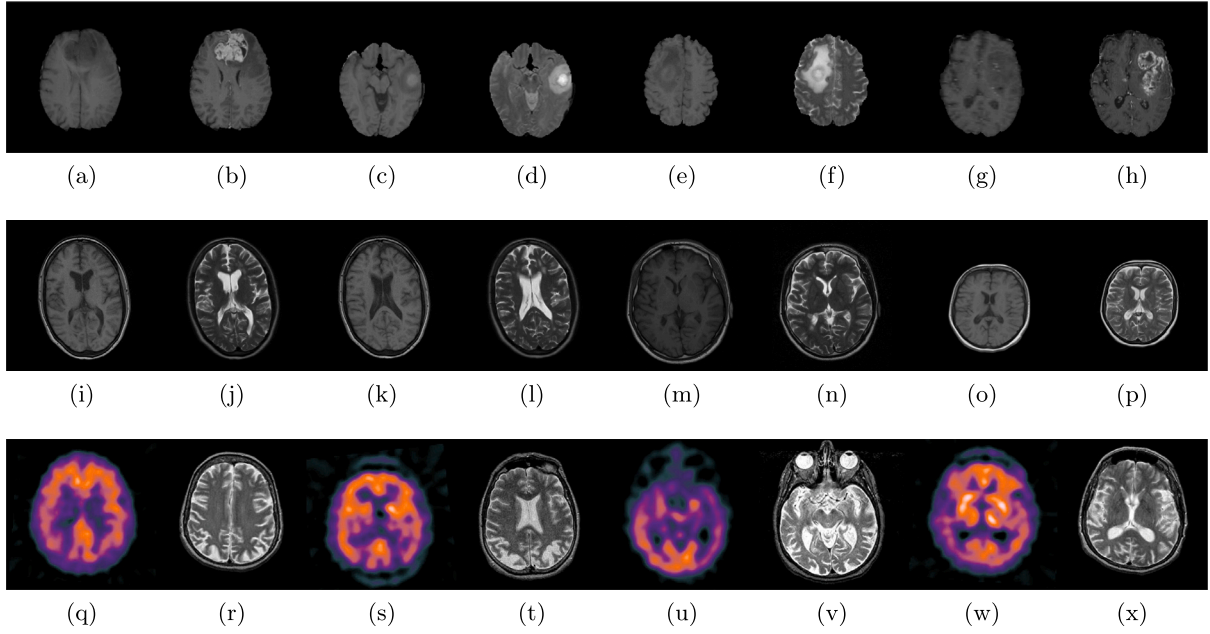


Fig. 2. Input images:(a-h)-Dataset-1:(a,b)-Pair-1, (c,d)-Pair-2, (e,f)-Pair-3, (g,h)-Pair-4; (i-p)-Dataset-2:(i,j)-Pair-5, (k,l)-Pair-6, (m,n)-Pair-7, (o,p)-Pair-8; (q-x)-Dataset-3:(q,r)-Pair-9, (s,t)-Pair-10, (u,v)-Pair-11, (w,x)-Pair-12.

where M_D is the final outcome of the fused image and $Mean = \frac{1}{A \times B} \sum_{a=1}^A \sum_{b=1}^B |M_D|$.

2. Universal image quality index (UIQI)

The distortion in the fused image is analyzed using the UIQI metric [31]. It is the combination of three components, namely correlation, luminance and contrast. The value of UIQI ranges between 0 to 1. If the value is high, it denotes less distortion in the image. For the input images M_1 , M_2 and the integrated output image M_D , it is formulated as

$$UIQI(M_1, M_2, M_D) = \frac{UIQI(M_1, M_D) + UIQI(M_2, M_D)}{2} \quad (20)$$

such that,

$$UIQI(M_1, M_D) = \frac{\sigma_{M_1 M_D}}{\sigma_{M_1} \sigma_{M_D}} \cdot \frac{2\bar{M}_1 \bar{M}_D}{\bar{M}_1^2 + \bar{M}_D^2} \cdot \frac{\sigma_{M_1} \sigma_{M_D}}{\sigma_{M_1}^2 + \sigma_{M_D}^2}$$

$$UIQI(M_2, M_D) = \frac{\sigma_{M_2 M_D}}{\sigma_{M_2} \sigma_{M_D}} \cdot \frac{2\bar{M}_2 \bar{M}_D}{\bar{M}_2^2 + \bar{M}_D^2} \cdot \frac{\sigma_{M_2} \sigma_{M_D}}{\sigma_{M_2}^2 + \sigma_{M_D}^2}$$

where $\bar{M}_1, \bar{M}_2, \bar{M}_D$ represents mean of M_1, M_2, M_D respectively. $\sigma_{M_1}^2, \sigma_{M_2}^2, \sigma_{M_D}^2$ denotes the variance of M_1, M_2, M_D respectively. $\sigma_{M_1 M_D}$ is the co-variance between M_1 and M_D .

3. Peak signal-to-noise ratio (PSNR)

The PSNR value determines the closeness of the fused image to that of the original images. The higher the value, the more information from the source images is carried over to the fused image. It is given as [31]

$$PSNR(M_1, M_2, M_D) = \frac{PSNR(M_1, M_D) + PSNR(M_2, M_D)}{2} \quad (21)$$

such that,

$$PSNR(M_1, M_D) = 10 \log_{10} \left(\frac{A \times B \times L^2}{\sum_{a=1}^A \sum_{b=1}^B (M_1(a, b) - M_D(a, b))^2} \right)$$

$$PSNR(M_2, M_D) = 10 \log_{10} \left(\frac{A \times B \times L^2}{\sum_{a=1}^A \sum_{b=1}^B (M_2(a, b) - M_D(a, b))^2} \right)$$

where L is the maximum gray-level value.

4. Average gradient (AG)

The AG [32] metric describes the clarity in the fused image concerning direction. For better fusion output, the value must be high. It is calculated as

$$AG = \frac{1}{A \times B} \sum_{a=1}^A \sum_{b=1}^B [(M_D(a, b) - M_D(a + 1, b))^2 + (M_D(a, b) - M_D(a, b + 1))^2]^{\frac{1}{2}} \quad (22)$$

5. Mutual information (MI)

The MI metric gives the measure of dependency of the fused image with source images. The value must be high for better fusion results. It is represented as [28]

$$MI(M_1, M_2, M_D) = \frac{MI(M_1, M_D) + MI(M_2, M_D)}{2},$$

$$MI(M_1, M_D) = \sum_{a=1}^A \sum_{b=1}^B p_{M_1 M_D}(a, b) \log \frac{p_{M_1 M_D}(a, b)}{p_{M_1}(a) p_{M_D}(b)}, \quad (23)$$

$$MI(M_2, M_D) = \sum_{a=1}^A \sum_{b=1}^B p_{M_2 M_D}(a, b) \log \frac{p_{M_2 M_D}(a, b)}{p_{M_2}(a) p_{M_D}(b)},$$

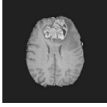
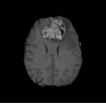
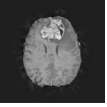
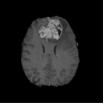
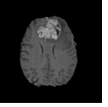
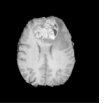
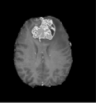
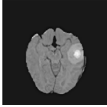
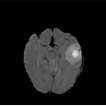
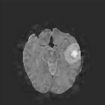
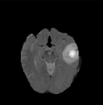
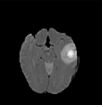
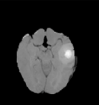
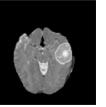
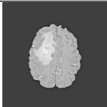
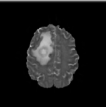

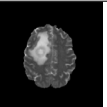
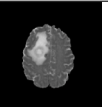
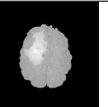
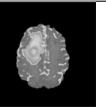
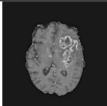
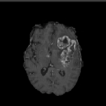
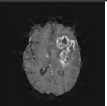
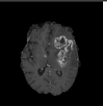
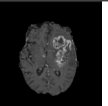
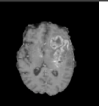
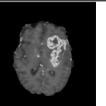
where p_{M_1} and p_{M_2} are marginal probability distribution of original images. And, $p_{M_1 M_D}$ and $p_{M_2 M_D}$ is the normalized joint distributions.

4.4. Qualitative and quantitative assessment

The fused output image is evaluated in two ways: qualitative and quantitative assessment. The qualitative assessment is visual quality based on the interpretation of humans in analyzing the outcome, while the quantitative assessment is a measurable value obtained from the fusion metrics. Both assessment is necessary to determine the efficiency of the fusion methods. Moreover, the complexity of the fused techniques is also studied by calculating the time for the execution of the processes. As mentioned, the experiment for 4 pairs of each dataset is shown for the proposed and other comparative methods. The subjective and objective analysis results for each dataset are tabulated and presented in Tables 2–4. The highest value of the fusion metric and the lowest time consumption are highlighted in bold.

The dataset-1 consists of T1-weighted and T2-weighted glioma images. Glioma is one of the predominant primary brain tumors with less

Table 2
Subjective and objective results for dataset-1.

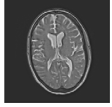
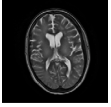

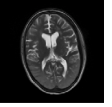
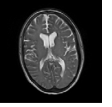
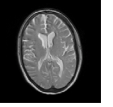
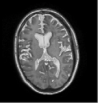
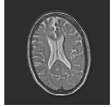
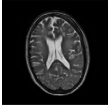
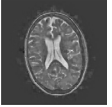
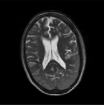
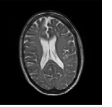
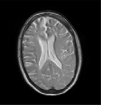
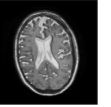
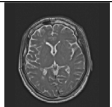
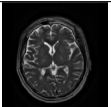
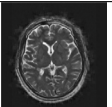
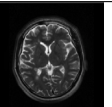
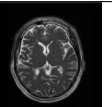
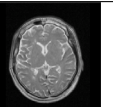
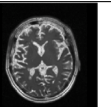

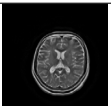
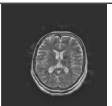




Fusion results for Pair-1							
Metrics \ Methods	EBFS-ICA	BM-PCNN-NSST	CS-MCA	MF-MBEMD	FGF-XDoG	SIFS	Proposed
SD	14.2240	33.9123	25.0605	38.4623	43.8921	50.76500	56.8552
UIQI	0.4197	0.7284	0.4537	0.7534	0.8249	0.6301	0.9711
PSNR	10.6467	23.6417	14.3870	23.7893	23.9218	21.8567	24.5193
AG	1.1612	6.6234	1.5702	7.4325	7.8138	4.5042	9.3561
MI	0.1165	2.7612	1.0586	2.9238	3.0127	3.1375	3.5315
TIME (s)	4.2978	51.0231	203.8721	5.9142	7.1228	3.3839	5.8281
OUTPUT							
Fusion results for Pair-2							
Metrics \ Methods	EBFS-ICA	BM-PCNN-NSST	CS-MCA	MF-MBEMD	FGF-XDoG	SIFS	Proposed
SD	32.3256	40.5995	35.3173	42.0632	45.2813	58.6231	62.3693
UIQI	0.1825	0.7124	0.2674	0.8045	0.8572	0.3244	0.9627
PSNR	14.3396	24.8330	15.5170	25.3702	26.1982	16.2134	27.1247
AG	1.1703	2.8357	1.1827	3.2602	3.8105	1.8073	4.9017
MI	0.2115	2.2322	1.8723	2.3883	2.4671	2.5180	2.9234
TIME (s)	4.7831	50.7381	201.7321	5.8997	6.2348	3.1659	5.7837
OUTPUT							
Fusion results for Pair-3							
Metrics \ Methods	EBFS-ICA	BM-PCNN-NSST	CS-MCA	MF-MBEMD	FGF-XDoG	SIFS	Proposed
SD	13.1492	40.6294	27.5322	43.7219	45.8136	63.1183	59.7821
UIQI	0.3472	0.8489	0.3711	0.8642	0.8979	0.4005	0.9274
PSNR	9.9363	19.4871	12.4847	19.9831	20.2763	13.8810	21.1938
AG	0.7838	4.3167	2.6803	4.2782	4.5012	2.8305	5.7410
MI	0.3457	1.9031	1.8873	2.0671	2.1652	2.1868	2.7503
TIME (s)	3.9958	49.9014	198.9312	5.2842	5.9567	3.0452	4.9865
OUTPUT							
Fusion results for Pair-4							
Metrics \ Methods	EBFS-ICA	BM-PCNN-NSST	CS-MCA	MF-MBEMD	FGF-XDoG	SIFS	Proposed
SD	12.2793	32.9402	21.0442	35.7302	38.2314	50.5619	70.9565
UIQI	0.4218	0.8525	0.4390	0.8767	0.8924	0.5298	0.9681
PSNR	12.5299	20.2579	14.3001	21.8434	22.4812	17.6594	24.8046
AG	1.6400	4.8477	2.2132	5.3298	6.0149	2.9039	12.3192
MI	0.2761	2.8548	1.5436	2.9743	3.0168	3.0825	3.3725
TIME (s)	5.0712	54.7419	204.1710	6.1632	7.8531	3.3845	5.9278
OUTPUT							

survival rate; thus, attention is needed to treat it. The T1-weighted MR gives the details of the soft tissues, whereas the T2-weighted MR concentrates more on the tumor information. Thus, a fusion of both images is used in diagnosing the disorder. The subjective and objective fusion results of this dataset, along with the running time in seconds, are given in the Table 2. It is noted that the outcome of the EBFS-ICA fusion algorithm has poor quality with blurry and low-contrast tumor images. Also, the tumor details are not appropriate to the source image. While considering the metric values, all the values are very low compared to the proposed method. Further, it has less time complexity which is appreciable, but the subjective and objective quality is not good. Thereafter, the fusion outcomes of the BM-PCNN-NSST method shows the better performance in merging the complementary information of the input images but lacks in retrieve the edge information of the tumor. Meanwhile, the objective metric values are moderate compared to other fusion methods and require more time for the execution of the algorithm. Then, it is noted that the resultant fusion image of the CS-MCA algorithm has some unwanted artifacts and degradation of spatial resolution. So, the tumor information is disturbed, and it leads

to inaccurate identification. Also, the metric values are not up to the mark, and this fusion method takes more time to accomplish the fusion process. Subsequent analysis of the fusion results obtained from the MF-MBEMD method highlights a limitation in accurately representing the contour details of the tumor image. Further, this algorithm yields moderately good objective metrics and improves computational efficiency. Afterwards, the results generated by the FGF-XDoG technique exhibit adequate fusion outcomes compared to the previously discussed methods. However, it struggles to capture minute details within the tumor image. Although the metric values are satisfactory, this technique exhibits moderately higher computational time. Next, SIFS produces fusion results with very high brightness, which leads to indistinguishable brain tumor regions and suppresses the edge details. Due to this high brightness, some of the objective value is increased, but it cannot be considered as a good result. Moreover, the processing time is low than other fusion methods. Finally, on analyzing the fusion result of the NETMMF method, all the information is transferred correctly such that curves and edges of the tumor are preserved. All the metric values are comparatively high, and the algorithm consumes moderate time.

Table 3

Subjective and objective results for dataset-2.

Fusion results for Pair-5							
Metrics \ Methods	EBFS-ICA	BM-PCNN-NSST	CS-MCA	MF-MBEMD	FGF-XDoG	SIFS	Proposed
SD	19.8836	55.6899	38.7690	56.2523	56.9982	58.1996	66.3322
UIQI	0.3541	0.7325	0.3800	0.7834	0.8124	0.6033	0.8931
PSNR	12.5009	16.9667	12.5331	17.382	17.9265	14.5099	19.5204
AG	2.9191	8.7102	4.1194	8.9725	9.7834	7.8464	10.6011
MI	0.3436	3.7201	2.7840	3.9316	4.1093	3.5510	4.5515
TIME (s)	4.8753	54.6628	210.8625	5.8932	6.5296	4.1639	5.6922
OUTPUT							
Fusion results for Pair-6							
Metrics \ Methods	EBFS-ICA	BM-PCNN-NSST	CS-MCA	MF-MBEMD	FGF-XDoG	SIFS	Proposed
SD	18.3626	58.0629	36.2865	58.2679	58.4816	58.5171	65.4344
UIQI	0.3817	0.73035	0.4778	0.7947	0.8278	0.6131	0.8800
PSNR	12.2169	18.4117	14.5512	18.6343	18.7892	16.5257	18.9495
AG	2.4394	8.7612	3.7533	8.9342	9.1564	7.2137	10.1834
MI	0.3287	3.4487	2.7782	3.8427	3.9783	3.3925	4.4766
TIME (s)	5.4218	56.7842	206.0862	6.9973	7.5317	3.7528	6.6439
OUTPUT							
Fusion results for Pair-7							
Metrics \ Methods	EBFS-ICA	BM-PCNN-NSST	CS-MCA	MF-MBEMD	FGF-XDoG	SIFS	Proposed
SD	15.6098	49.9230	28.4557	50.1632	52.8932	49.1353	58.5758
UIQI	0.1600	0.7309	0.2400	0.7856	0.7974	0.5035	0.8070
PSNR	13.4093	17.2720	14.2577	17.8729	18.1921	16.9207	18.8807
AG	2.7488	9.4233	3.7957	9.7192	9.9821	7.9985	10.7605
MI	0.2305	4.1723	2.1822	4.3802	4.5829	3.9564	4.9854
TIME (s)	4.6346	53.9724	208.1489	5.8272	6.4128	4.0321	5.1944
OUTPUT							
Fusion results for Pair-8							
Metrics \ Methods	EBFS-ICA	BM-PCNN-NSST	CS-MCA	MF-MBEMD	FGF-XDoG	SIFS	Proposed
SD	15.0989	52.5702	32.4054	52.9273	53.1389	53.5702	67.6399
UIQI	0.3231	0.7352	0.3984	0.7635	0.8127	0.5944	0.8924
PSNR	13.6377	17.309	14.6055	17.9235	18.4387	17.1317	19.9830
AG	2.0507	8.4341	4.1225	8.9956	9.3219	7.1728	10.4165
MI	0.2662	2.8034	1.9877	2.9281	3.0112	2.9323	3.1761
TIME (s)	4.9897	52.4912	201.6002	6.4265	7.3094	2.9648	6.0136
OUTPUT							

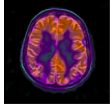
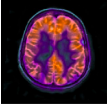
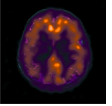

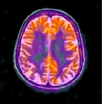
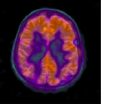
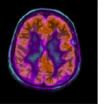
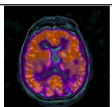
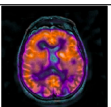
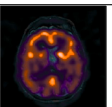
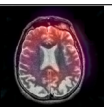

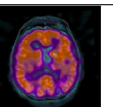
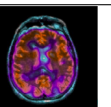
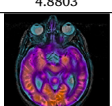
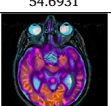
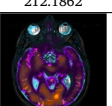


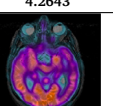
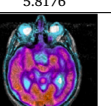
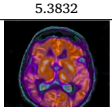
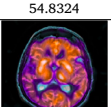
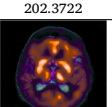
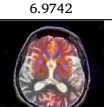
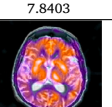
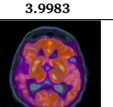
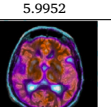
The T1-weighted MR and T2-weighted MR images of multiple sclerosis are taken in dataset-2. Multiple sclerosis is a chronic autoimmune disorder that affects the central nervous system. Identifying multiple sclerosis lesions through a single imaging modality is difficult. So, the fused image aids in better diagnosis. For this purpose, the experiment is done for this dataset, and the results with time consumption are tabulated in Table 3. First, on noticing the result of the EBFS-ICA fusion technique, it produces unsatisfactory results with inadequate information. Even though it has less computational time, the visual quality and metric values are not standard. Second, the BM-PCNN-NSST fusion method fuses the information without distortion, but the contour details are missing. Moreover, the objective metric values are not sufficiently good, and the algorithm takes more running time. Third, it is observed that the fusion results of the CS-MCA algorithm are surrounded by an unwanted noise which decreases the quality of the image. Besides, only the average values are obtained for the fusion metrics compared to other fusion methods. Also, this algorithm consumes more time for execution than all other comparative fusion methods. Fourth, the fusion outcome generated by the MF-MBEMD

method deteriorates the spatial relationship between structures and abnormalities. Despite this limitation, the method yields acceptable values when objectively assessing the metrics. Moreover, the execution time of this algorithm is relatively minimal. Fifth, the FGF-XDoG fusion technique effectively retains all features from the input images without feature loss but fails to portray intricate details. While the metric evaluations commend its performance, the higher time consumption when executing the algorithm is the drawback. Sixth, the fusion outcome of the SIFS method has less capacity to differentiate the varying intensities, so information is not identified properly. In addition, the objective values are not high, but the time consumption in executing the algorithm is comparatively good. Finally, the proposed NETMMF fusion results provide all the texture features of the input images with clarity and high contrast. Also, the highest fusion metric value is obtained for the resultant fused image. The time consumption in performing this algorithm is average compared to other methods.

Alzheimer's disease is taken in dataset-3 as it is one of the serious disorders of the brain that needs more attention. It is a neurodegenerative disease that causes dementia in patients. Thus, a fusion of

Table 4

Subjective and objective results for dataset-3.

Fusion results for Pair-9							
Metrics \ Methods	EBFS-ICA	BM-PCNN-NSST	CS-MCA	MF-MBEMD	FGF-XDoG	SIFS	Proposed
SD	17.2854	54.1917	28.4557	32.6765	40.4366	44.3216	68.8909
UIQI	0.3452	0.62023	0.4215	0.4387	0.4546	0.4766	0.8067
PSNR	11.3684	16.9778	13.5449	13.6547	14.2046	14.0201	20.5040
AG	1.8142	9.6148	2.2867	7.3285	7.5483	8.6701	13.1028
MI	0.3592	3.4980	1.1460	1.3648	1.4371	1.7832	3.0472
TIME (s)	4.9298	57.8261	216.9371	6.2349	6.9636	4.7103	5.9821
OUTPUT							
Fusion results for Pair-10							
Metrics \ Methods	EBFS-ICA	BM-PCNN-NSST	CS-MCA	MF-MBEMD	FGF-XDoG	SIFS	Proposed
SD	13.4854	57.9812	18.5871	41.8244	43.8935	40.8136	62.8685
UIQI	0.2625	0.6014	0.3449	0.4473	0.4503	0.4627	0.7713
PSNR	10.2533	14.9318	11.8457	10.4832	12.2452	13.0170	18.5873
AG	3.8900	5.5023	4.9960	7.4672	7.9835	8.6611	12.2547
MI	0.3960	3.6821	1.0537	1.6943	1.7183	2.9218	3.7235
TIME (s)	5.2721	52.8912	198.7832	6.2245	6.8263	3.7321	5.8292
OUTPUT							
Fusion results for Pair-11							
Metrics \ Methods	EBFS-ICA	BM-PCNN-NSST	CS-MCA	MF-MBEMD	FGF-XDoG	SIFS	Proposed
SD	20.7563	57.9546	30.1395	48.876	49.6271	48.0644	72.6803
UIQI	0.3745	0.6902	0.4870	0.5129	0.5326	0.5032	0.8348
PSNR	8.9890	12.3034	9.7809	10.2315	10.7437	10.8564	17.8744
AG	2.2467	14.4454	4.9391	9.5368	9.8463	10.0277	17.8536
MI	0.1954	2.5843	0.8926	1.0564	1.1439	1.2238	2.8693
TIME (s)	4.8803	54.6931	212.1862	6.1694	6.4593	4.2643	5.8176
OUTPUT							
Fusion results for Pair-12							
Metrics \ Methods	EBFS-ICA	BM-PCNN-NSST	CS-MCA	MF-MBEMD	FGF-XDoG	SIFS	Proposed
SD	15.9356	60.3719	21.7556	45.7393	46.3751	44.8043	69.1767
UIQI	0.3616	0.7009	0.4278	0.5074	0.5275	0.5916	0.8741
PSNR	10.3258	15.2748	12.2356	13.4356	13.6649	13.7650	17.9032
AG	3.9903	10.8809	5.3794	8.6431	8.9648	9.0243	13.5379
MI	0.4610	3.8436	1.2351	1.7546	2.0164	2.9863	3.9813
TIME (s)	5.3832	54.8324	202.3722	6.9742	7.8403	3.9983	5.9952
OUTPUT							

images obtained from SPECT and T2-weighted MR imaging modalities is used in diagnosing this problem. The subjective and objective results of this dataset are displayed in the Table 4. The EBFS-ICA fusion algorithm is not suitable for this dataset since it produces undesirable artifacts and makes the obscured fused image. Likewise, the objective value is meagre compared to the methods. It is observed that the time taken to accomplish the fusion algorithm for this dataset is slightly higher than the time taken for the previous two datasets. Afterwards, the resultant fusion image produced by the BM-PCNN-NSST method has all the complementary information from the input images but some of redundant information adhering to it. Further, it has reasonable fusion metric value and time consumption. Then, the CS-MCA fusion technique provides poor result in which all the information of the source images are lost. Although it takes less time to compute, the subjective and objective quality is not good. After that, the fusion outcomes generated by MF-MBEMD fail to incorporate the functional data acquired from the SPECT modalities, resulting in subpar fusion results. Furthermore, these outcomes exhibit lower metric values than the results obtained for the other two datasets. Nevertheless, the execution time for the algorithm remains consistent across all three datasets.

Then, upon reviewing the fusion output of the FGF-XDoG method, it becomes evident that the information derived from T2-weighted MR imaging modalities takes precedence over the information obtained from SPECT modalities, resulting in an imbalance. Furthermore, the metric values fall below the expected standard. Regarding execution time, the method delivers only intermediate performance. Next, in the results of the SIFS fusion method, unclear and blurred structures are identified. It has a moderate fusion metric value and has less time consumption than other methods. Lastly, the fusion outcome of the proposed NETMMF method has detailed information with clear boundaries. It gives the highest metric values and has reasonable time consumption.

4.5. Discussion

Here, in this subsection, the obtained experimental results are deliberated precisely. First, the SD metric value in pair-3 is higher for the SIFS fusion method than the proposed fusion method. The reason is the over-enhanced fused image obtained from the SIFS fusion method.

Table 5

Average running time for every fusion methods on each dataset.

Methods Datasets	Size	EBFS-ICA	BM-PCNN-NSST	CS-MCA	MF-MBEMD	FGF-XDoG	SIFS	Proposed
Dataset-1	240 × 240	4.5369	51.6011	202.1766	5.8153	6.7918	3.2448	5.6315
Dataset-2	256 × 256	4.9804	54.4776	206.6744	6.2861	6.9458	3.7284	5.8877
Dataset-3	256 × 256	5.1164	55.0607	207.566	6.4007	7.02234	4.17625	5.9061

However, the features are indistinguishable, and thus it cannot be considered an excellent fused output image. In comparison, the proposed NETMMF method produces a fused image with high visual quality and preserved edges. Likewise, in pair-9, the MI metric value for the BM-PCNN-NSST method is higher than the proposed method. This is because BM-PCNN-NSST contains all the information from the source images. But, some noise is produced in the fused image that degrades the quality of the image. In contrast, the proposed fusion method gives a better outcome regarding edges, and no artifacts are present. Further, considering the time consumption, the proposed fusion method is always lacking behind SIFS and EBFS-ICA fusion methods. But, it is reasonable as it has little difference. For a more comprehensive analysis, the average running times for every fusion method on each dataset were individually calculated and presented in Table 5. The observations indicate a consistent increase in running time for all fusion methods when the dimension is increased or when color image is involved. In addition, the proposed method consistently secures the third position regarding time consumption. This is due to slightly higher complexities in executing the proposed NETMMF algorithm than SIFS and EBFS-ICA. Besides, all other metric values are high for the proposed fusion method in every pair. Also, it provides better visual quality with detailed edge information and noise-free result. Therefore, on the whole, the proposed NETMMF method is superior to other methods in the aspects of qualitative and quantitative assessments.

5. Conclusion

The proposed NETMMF method is framed to eliminate incompleteness and impreciseness in medical images. This challenge is accomplished by transferring the crisp images into neutrosophic images with the help of the three domains of neutrosophic sets. Then, the contour details of the images are acquired using the developed entropy. Further, the coarseness and contrast of the Tamura features are employed to extract the requisite features from the truth and entropy image. At last, the fusion is carried out using the information from these feature values and the fusion rule. Thus, the fused image has a clear texture feature, high contrast, and well-defined edge details. And most importantly, no unwanted artifacts and noises are included during the execution of this process. Moreover, the experimental results with three brain datasets for the proposed method and the other six comparative methods prove the efficacy of the proposed fusion method. Thus, the NETMMF fusion results demonstrate remarkable performance by encompassing all texture features from the input images with high clarity and enhanced contrast. The resultant fused image attains the highest metric value among comparative methods, indicating superior fusion quality. Further, regarding computational efficiency, the algorithm performs sufficiently within an average time consumption compared to alternative methods. In future, the neutrosophic medical image segmentation algorithm will be developed with the aid of this fusion method.

Ethical approval

This article does not contain any studies with human participants performed by any of the authors.

CRediT authorship contribution statement

K.G. Lavanya: Conceptualization, Formal analysis, Investigation, Methodology, Software, Validation, Visualization, Writing – original draft. **P. Dhanalakshmi:** Conceptualization, Formal analysis, Investigation, Methodology, Supervision, Writing – review & editing. **M. Nandhini:** Conceptualization, Formal analysis, Funding acquisition, Investigation, Methodology, Validation, Visualization, Writing – original draft.

Declaration of competing interest

The authors declare that they have no known competing financial interests or personal relationships that could have appeared to influence the work reported in this paper.

Data availability

Data will be made available on request.

Acknowledgment

This paper is partly supported by University Grants Commission (UGC), Department of Higher Education, Government of India through SJSGC Fellowship vide UGC scholarship ID No. 202223-UGCES-22-OB-TAM-F-SJSGC-9475.

References

- [1] A.A. Abdulla, Efficient computer-aided diagnosis technique for leukaemia cancer detection, *IET Image Process.* 14 (17) (2020) 4435–4440, <http://dx.doi.org/10.1049/iet-ipr.2020.0978>.
- [2] W. Tang, F. He, Y. Liu, Y. Duan, MATR: Multimodal medical image fusion via multiscale adaptive transformer, *IEEE Trans. Image Process.* 31 (2022) 5134–5149, <http://dx.doi.org/10.1109/TIP.2022.3193288>.
- [3] D. Palanisami, N. Mohan, L. Ganeshkumar, A new approach of multi-modal medical image fusion using intuitionistic fuzzy set, *Biomed. Signal Process. Control* 77 (2022) 103762, <http://dx.doi.org/10.1016/j.bspc.2022.103762>.
- [4] R. Panda, S. Agrawal, EBFS-ICA: An efficient algorithm for CT-MRI image fusion, in: *SEMCCO 2010, LNCS 6466*, Springer Verlag, 2010, pp. 356–361, http://dx.doi.org/10.1007/978-3-642-17563-3_43.
- [5] S. Singh, H. Singh, A. Gehlot, J. Kaur, Gagandeep, IR and visible image fusion using DWT and bilateral filter, *Microsyst. Technol.* 29 (4) (2023) 457–467, <http://dx.doi.org/10.1007/s00542-022-05315-7>.
- [6] H.M. El-Hoseny, W.Abd. El-Rahman, E.S.M. El-Rabaie, F.E. Abd El-Samie, O.S. Faragallah, An efficient DT-CWT medical image fusion system based on modified central force optimization and histogram matching, *Infrared Phys. Technol.* 94 (2018) 223–231, <http://dx.doi.org/10.1016/j.infrared.2018.09.003>.
- [7] Q. Xie, J. Hu, X. Wang, D. Zhang, H. Qin, Novel and fast EMD-based image fusion via morphological filter, *Vis. Comput.* 39 (9) (2023) 4249–4265, <http://dx.doi.org/10.1007/s00371-022-02588-x>.
- [8] W. Tan, P. Tiwari, H.M. Pandey, C. Moreira, A.K. Jaiswal, Multimodal medical image fusion algorithm in the era of big data, *Neural Comput. Appl.* (2020) 1–21, <http://dx.doi.org/10.1007/s00521-020-05173-2>.
- [9] Y. Jie, X. Li, F. Zhou, H. Tan, Medical image fusion based on extended difference-of-Gaussians and edge-preserving, *Expert Syst. Appl.* 227 (2023) 120301, <http://dx.doi.org/10.1016/j.eswa.2023.120301>.
- [10] Y. Liu, X. Chen, R.K. Ward, Z.J. Wang, Medical image fusion via convolutional sparsity based morphological component analysis, *IEEE Signal Process. Lett.* 26 (3) (2019) 485–489, <http://dx.doi.org/10.1109/LSP.2019.2895749>.
- [11] J. Zhang, Q. Qin, Q. Ye, T. Ruan, ST-unet: Swin transformer boosted U-net with cross-layer feature enhancement for medical image segmentation, *Comput. Biol. Med.* 153 (2023) 106516, <http://dx.doi.org/10.1016/j.combiomed.2022.106516>.
- [12] L.A. Zadeh, Fuzzy sets, *Inf. Control* 8 (3) (1965) 338–358.

- [13] M. Manchanda, R. Sharma, A novel method of multimodal medical image fusion using fuzzy transform, *J. Vis. Commun. Image Represent.* 40 (2016) 197–217, <http://dx.doi.org/10.1016/j.jvcir.2016.06.021>.
- [14] K.T. Atanassov, Intuitionistic fuzzy sets, *Fuzzy Sets and Systems* 20 (1) (1986) 87–96.
- [15] T. Tirupal, B.C. Mohan, S.S. Kumar, Multimodal medical image fusion based on Sugeno's intuitionistic fuzzy sets, *ETRI J.* 39 (2) (2017) 173–180, <http://dx.doi.org/10.4218/etrij.17.0116.0568>.
- [16] F. Smarandache, *Neutrosophy: Neutrosophic Probability, Set, and Logic: Analytic Synthesis & Synthetic Analysis*, 1998, p. 105.
- [17] H. Wang, F. Smarandache, Y. Zhang, R. Sunderraman, Single valued neutrosophic sets, in: *Proceedings of 10th International Conference on Fuzzy Theory and Technology*, 2005, pp. 410–413.
- [18] R. Premalatha, P. Dhanalakshmi, Robust neutrosophic fusion design for magnetic resonance (MR) brain images, *Biomed. Signal Process. Control* 84 (2023) 104824, <http://dx.doi.org/10.1016/j.bspc.2023.104824>.
- [19] N. Nagaraja Kumar, T. Jayachandra Prasad, K.S. Prasad, An intelligent multimodal medical image fusion model based on improved fast discrete curvelet transform and type-2 fuzzy entropy, *Int. J. Fuzzy Syst.* 25 (1) (2023) 96–117, <http://dx.doi.org/10.1007/s40815-022-01379-9>.
- [20] P. Majumdar, S.K. Samanta, On similarity and entropy of neutrosophic sets, *J. Intell. Fuzzy Systems* 26 (3) (2014) 1245–1252, <http://dx.doi.org/10.3233/IFS-130810>.
- [21] P. Singh, A neutrosophic-entropy based adaptive thresholding segmentation algorithm: A special application in MR images of Parkinson's disease, *Artif. Intell. Med.* 104 (2020) 101838, <http://dx.doi.org/10.1016/j.artmed.2020.101838>.
- [22] X. Bian, H. Pan, K. Zhang, C. Chen, P. Liu, K. Shi, NeDSem: Neutrosophy domain-based segmentation method for malignant melanoma images, *Entropy* 24 (6) (2022) 783, <http://dx.doi.org/10.3390/e24060783>.
- [23] D. Napoleon, I. Kalaiarasi, Classifying lung cancer as benign and malignant nodule using ann of back-propagation algorithm and glcm feature extraction on chest X-ray images, *Wirel. Pers. Commun.* 126 (1) (2022) 167–195, <http://dx.doi.org/10.1007/s11277-022-09594-1>.
- [24] H. Tamura, S. Mori, T. Yamawaki, Textural features corresponding to visual perception, *IEEE Trans. Syst. Man Cybern.* 8 (6) (1978) 460–473, <http://dx.doi.org/10.1109/TSMC.1978.4309999>.
- [25] S. Xiaoming, Z. Ning, W. Haibin, Y. Xiaoyang, W. Xue, Y. Shuang, Medical image retrieval approach by texture features fusion based on Hausdorff distance, *Math. Probl. Eng.* 2018 (2018) 1–12, <http://dx.doi.org/10.1155/2018/7308328>.
- [26] M. Abdel-Basset, N.N. Mostafa, K.M. Sallam, I. Elgendi, K. Munasinghe, Enhanced COVID-19 X-ray image preprocessing schema using type-2 neutrosophic set, *Appl. Soft Comput.* 123 (2022) 108948, <http://dx.doi.org/10.1016/j.asoc.2022.108948>.
- [27] S. Bakas, H. Akbari, A. Sotiras, M. Bilello, M. Rozycki, J.S. Kirby, J.B. Freymann, K. Farahani, C. Davatzikos, Advancing the cancer genome atlas glioma MRI collections with expert segmentation labels and radiomic features, *Sci. Data* 4 (1) (2017) 1–13, <http://dx.doi.org/10.1038/sdata.2017.117>.
- [28] A.M. Muslim, S. Mashohor, G. Al Gawwam, R. Mahmud, M. binti Hanafi, O. Alnuaimi, R. Josephine, A.D. Almutairi, Brain MRI dataset of multiple sclerosis with consensus manual lesion segmentation and patient meta information, *Data Brief* 42 (2022) 108139, <http://dx.doi.org/10.1016/j.dib.2022.108139>.
- [29] K.A. Johnson, J.A. Becker, The Whole Brain Atlas. Available from: <http://www.med.harvard.edu/AANLIB/home.html>.
- [30] S. Li, B. Yang, J. Hu, Performance comparison of different multi-resolution transforms for image fusion, *Inf. Fusion* 12 (2) (2011) 74–84, <http://dx.doi.org/10.1016/j.inffus.2010.03.002>.
- [31] P. Bharti, D. Mittal, An ultrasound image enhancement method using neutrosophic similarity score, *Ultrason. Imaging* 42 (6) (2020) 271–283, <http://dx.doi.org/10.1177/0161734620961005>.
- [32] S. Daneshvar, H. Ghassemlian, MRI and PET image fusion by combining IHS and retina-inspired models, *Inf. Fusion* 11 (2) (2010) 114–123, <http://dx.doi.org/10.1016/j.inffus.2009.05.003>.